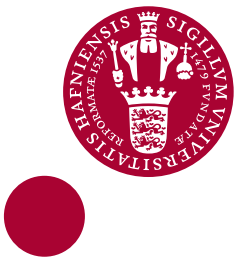

Comparison of precipitable water over Ghana using GPS signals and reanalysis products

Acheampong, A.A.; Fosu, C.; Amekudzi, L.K.; Kaas, Eigil

Published in:
Journal of Geodetic Science

DOI:
10.1515/jogs-2015-0016

Publication date:
2015

Document version
Publisher's PDF, also known as Version of record

Research Article **Open Access**

A. A. Acheampong*, C. Fosu, L. K. Amekudzi, and E. Kaas

Comparison of precipitable water over Ghana using GPS signals and reanalysis products

DOI 10.1515/jogs-2015-0016
Received January 9, 2015; accepted November 16, 2015

Abstract: Signals from Global Navigational Satellite Systems (GNSS) when integrated with surface meteorological parameters can be used to sense atmospheric water vapour. Using gLAB software and employing precise point positioning techniques, zenith troposphere delays (ZTD) for a GPS base station at KNUST, Kumasi have been computed and used to retrieve Precipitable Water (PW). The PW values obtained were compared with products from ERA-Interim and NCEP reanalysis data. The correlation coefficients, r, determined from these comparisons were 0.839 and 0.729 for ERA-interim and NCEP respectively. This study has demonstrated that water vapour can be retrieved with high precision from GNSS signal. Furthermore, a location map have been produced to serve as a guide in adopting and installing GNSS base stations in Ghana to achieve a country wide coverage of GNSS based water vapour monitoring.

Keywords: GNSS; integrated water vapour; numerical weather prediction; precipitable water; reanalysis model

1 Introduction

Climate change and variability are impacting greatly on human existence and the challenge for research is to understand the processes influencing such change. There are numerical weather predictions (NWP) models that have been used to study weather and climatic patterns (Lynch, 2008; Buizza, 2002; Shuman, 1978). These NWP models use winds, heat transfer, radiation, relative humidity and surface meteorological parameters as input to describe rising earth surface temperature, increasing greenhouse gases, precipitations, decreasing ice and other geophysical phenomena (Soos, 2010).

Unlike other greenhouse gases, water vapour coupled with its atmospheric concentration is not significantly influenced by direct anthropogenic activities (USGS, 2011; Seidel, 2002). This is because water vapour contributes to climate change through natural evolution and feedback mechanism. Again its contents in the atmosphere is highly variable both in space and in time due to temperature changes, atmospheric circulation and micro-physical processes (Pottiaux, 2010). According to Solomon et al. (2007), an estimated 70% of the recent rises in atmospheric temperature are attributed to water vapour feedback.

The amount and distribution of water vapour in space (horizontal and vertical) is a major parameter in the development of NWP models and its importance cannot be underestimated. Sensing and measurement of water vapour by conventional methods such as radiosondes, hygrometers, microwave radiometers, sun photometers are affected by meteorological conditions. In addition they are expensive and have coverage limitations. Again water vapour is under sampled in current operational meteorological and climate observing systems (Pichelli et al., 2010; Pierdicca et al., 2009; Gendt et al., 2003). Making available ne-resolution and accurate 2D and 3D water vapour field measurements would lead to substantial improvements in NWP model initialization (Sahoo et al., 2013).

Over two decades ago Global Navigation Satellite System (GNSS) signals were used to retrieve water vapour Bevis et al. (1992). The GNSS technique characterizes the propagation delays on the signals caused by the neutral atmosphere or troposphere and the magnitude of the delayed component is directly proportional to the atmospheric water vapour. This method is highly accurate irrespective of adverse meteorological conditions and with modeling capabilities to estimate errors with high temporal and spatial resolution. Moreover, GNSS receivers used in this application have little or no maintenance requirements and supports operational fore-casting of atmospheric conditions. This paper investigates how the GNSS meteorological concepts can be used to sense atmospheric water vapour to boost surface meteorological

***Corresponding Author: A. A. Acheampong:** Kwame Nkrumah University of Science and Technology, Kumasi, Ghana, E-mail: aaacheampong.coe@knust.edu.gh
C. Fosu, L. K. Amekudzi: Kwame Nkrumah University of Science and Technology, Kumasi, Ghana
E. Kaas: Niels Bohr Inst, University of Copenhagen, Denmark

parameters being observed in the Ghana Meteorological agency (GMet) network and improve weather prediction.

2 Methodology

Sensing meteorological parameters using GNSS signals can be achieved using either ground-based surface network of GNSS receivers or aboard low Earth orbiting satellites (De Haan and Van Der Marel, 2008). The later approach is known as radio occultation technique. For this work delayed signals due to tropospheric and stratospheric effects was used retrieved atmospheric Integrated Water Vapour (IWV).

Figure 1 gives an overview of the general concept. This technique is based on the precise determination of tropospheric[1] delays, an output of GNSS data processing (Bosy et al., 2011). When not mitigated tropospheric delays can introduce range errors of 2.3 m to 9.3 m for a satellite at the zenith down to 15° elevation angle, and about 20 - 28 m for those between 5o and observer horizon (Leick, 2003; El-Rabbany, 2002).

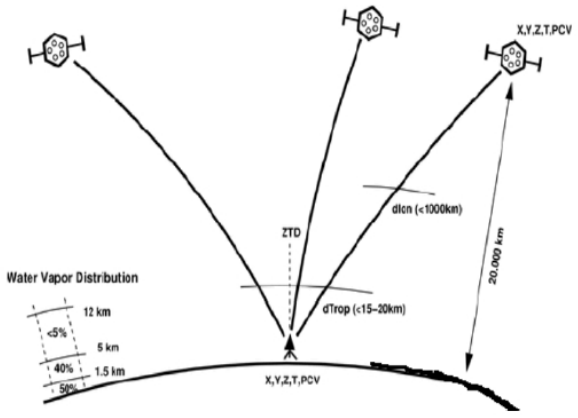

Figure 1: Water vapour distribution and atmospheric layers in relation to GNSS satellites. X; Y; Z are coordinates of satellites and antenna positions, T is the epoch of observation, PCV are phase center values of transmitting and receiving antenna, ZTD is the zenith tropospheric delays

2.1 Mathematical Models

Following Seeber (2003) the ideal delay observation equation would be:

$$\Delta R = R^{sat} - R_{rec}$$

where R^{sat} is the true distance from the satellite to the receiver and R_{rec} is equal to the actual recorded signal transit time multiplied by the speed of light in vacuum, c. However, in addition to the lower atmosphere contributing to the delay, several other processes influence the measured delay. So, considering all contributions to the observed code phase, p(t), Eq. (1) and carrier phase, φ(t), Eq. (2) the real situation can be formulated as

$$p(t) = R_r^s + c[\delta t^s - \delta t_r] + d_{ion} + \Delta L_a^i(\epsilon) + \zeta + d_{orb} \quad (1)$$

$$\varphi(t) = R_r^s + c[\delta t^s - \delta t_r] + \lambda\eta - d_{ion} + \Delta L_a^i(\epsilon) + \zeta + d_{orb} \quad (2)$$

where:
R_r^s – Receiver Satellite distance in vacuum - Satellite and receiver position need to be accurately known;
$\delta t^s - \delta t_r$ – Satellite and receiver clock errors - Eliminated using double differences or precise IGS clock products;
η – Unknown initial phase ambiguities - Needs to be resolve into either fixed integer or float;
d_{ion} – Ionospheric delay - Eliminated using dual frequency ionosphere-free combination;
c – speed of light in vacuum;
λ, d_{orb}, ζ – wavelength of the carrier phase, orbital errors and excess noise from receivers vicinity;
$\Delta L_a^i(\epsilon)$ – Tropospheric delays at elevation angles, ϵ – Elevation angles.

The main differences between the code and carrier phases observables are for the wavelengths, carrier phases are shorter than code phases. Measurement noises are also small for carriers than code phases. There are ambiguities to be resolved in carrier measurements and the ionospheric propagation delays the code measurements but advances the carrier measurements.

For the purposes of GNSS meteorology, greater emphasis is given to the slant tropospheric delays, which are converted to zenith tropospheric delays (ZTD) using appropriate mapping functions (Bohm et al., 2006; Niell, 1996), when all other errors have been dealt with. The zenith tropospheric delays can be split into two components, the zenith hydrostatic delays (ZHD) and zenith wet delays (ZWD).

$$ZTD = ZHD + ZWD \quad (3)$$

1 Actually the delays also include a very small contribution from the stratosphere.

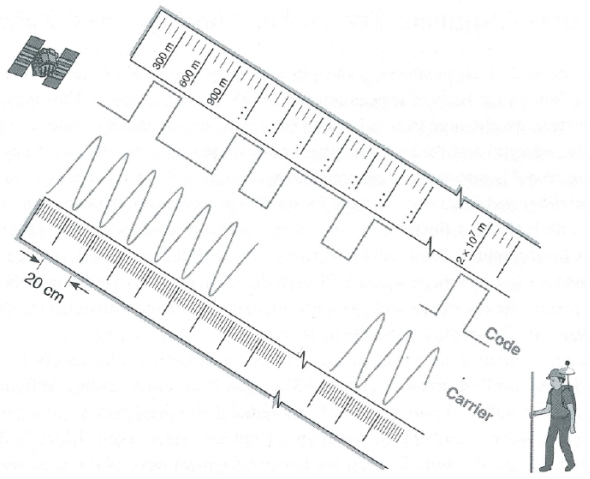

Figure 2: Conceptual representation of code and carrier phase measurements with a measuring tape (Misra and Enge, 2011)

IWV and Precipitable Water (PW) can then be retrieved from the computed ZWD values. The ZTD is the same as $\Delta L_a^i\ (\varepsilon)$ mapped onto the zenith. They are computed by first considering ray bending due to refractivity of the atmospheric medium making actual path taken by the signal greater than the geometric path as shown in Ning (2012); Schuler (2006); Bevis et al. (1992); Elgered et al. (1991):

$$\Delta L_a^i = \int_{atm} n(s) \cdot ds - \int_{vac} ds \tag{4}$$

where, ΔL_a^i is total slant delay from satellite, i to receiver's antenna, a, at elevation angle , ε; n is index of atmospheric refraction; ds is differential increment in distance with respect to the line of sight; $_{atm}$ and $_{vac}$ are atmospheric and vacuum media.

Expressing n in terms of refractivity N, which is the sum of refractivities of the dry gases and water vapour in the atmosphere, where $N = 10^6(n-1)$, and ignoring all other terms which are zero in the zenith direction, Eq. (4) becomes:

$$\Delta L_a^i(\epsilon) = 10^{-6} \int_{atm} N(s) \cdot ds = 10^{-6} \int_{atm} [N_d(s) + N_w(s)] \cdot ds \tag{5}$$

The refractivity of the atmosphere is a function of its temperature, pressure, water pressure and independent to microwave frequencies below 40 GHz (Nilsson et al., 2013). Thayer (1974) expressed N as

$$N = k_1 \frac{p_d}{T} Z_d^{-1} + k_2 \frac{e}{T} Z_w^{-1} + k_3 \frac{e}{T^2} Z_w^{-1} \tag{6}$$

where p_d and e are partial pressures of the dry gases and water vapour in hPa, T is absolute temperature in Kelvins; Z_d^{-1} and Z_w^{-1} are inverse are compressibility factors for dry and moist air respectively and are used to describe the deviation of the atmospheric constituents from an ideal gas; k_1, k_2 and k_3 are constants based on laboratories estimates and Bevis et al. (1994) found them to be k_1 = 77.60 ±0.05 K/hPa, k_2 = 77.40 ± 2.2 K/hPa, k_3 = 373900 ± 1200 K^2/hPa and k_2' = 22.10 ± 2.2 K/hPa. The compressibility factor as shown in Nilsson et al. (2013) for ideal gas, Z = 1, and other j^{th} constituent of air is given by:

$$Z_j = \frac{pM_j}{\rho_j RT}$$

where is M_j is the molar mass and R is the universal gas constant. From Eq. (6) the first term is ZHD, caused by the induced dipole moment of the dry gases and the remaining terms are ZWD, caused by the water vapour molecules (Ning, 2012).

From the equation of state for ideal gases, we found out that $p_d/T = R_d\rho_d$, where, R_d is the specific gas constant of the dry constituent, ($R_d = R/M_d$, R is the universal gas constant and M_d is the molar mass of the dry gases). Using simple approximations and the assumption of hydrostatic equation being valid for total pressure and not for partial pressures Davis et al. (1985) reformatted Eq. (6) to be:

$$N = k_1 R_d \rho + k_2' \frac{e}{T} + k_3 \frac{e}{T^2} \tag{7}$$

k_2' which has been given earlier is derived by $k_2' = k_2 - (M_w/M_d)k_1$ and M_w is the molar mass of water vapour; ρ is the total density of dry gases and water vapour.

When all the slant delays are mapped onto the zenith direction, zenith hydrostatic delays, $ZHD = \Delta L_d^z$ can be obtained by considering the assumption that hydrostatic equilibrium have been satisfied (Davis et al., 1985);

$$\frac{dp}{dh} = -\rho(h)g(h) \tag{8}$$

where g is the acceleration due to gravity in the vertical direction; p is the total pressure. The resultant integration of the first term in Eq. (7) gives:

$$\Delta L_d^z = (10^{-6} k_1 R_d g_m^{-1}) \cdot P_s \tag{9}$$

where P_s is the total ground pressure in hPa, g_m is gravitational acceleration at the mass centre of a vertical column of the atmosphere. Saastamoinen (1972) defines g_m = $(9.784 \pm 0.001\ \mathrm{m/s^2}) \cdot f(\theta, H)$, and $f(\theta, H) = (1 - 2.66 \cdot 10^{-3}\cos(2\theta) - 2.8 \cdot 10^{-7}H)$. The parameters θ and H are the latitude of the site in degrees and surface height above the geoid in meters respectively.

Substituting all the constants in Eq. (9), the expression for solving ZHD in units of length becomes:

$$\Delta L_d^z = 0.002277(1 + 0.0026\cos 2\theta + 0.00028H) \cdot P_s. \tag{10}$$

2.2 Precipitable Water Computation

The software gLAB® (Hernandez-Pajares et al., 2010) outputs the slant delays mapped onto the zenith. With ZTD already computed and knowledge of precise the coordinates of the antenna position (θ, H) and surface pressure values from nearby weather station, $ZWD = \Delta L_w^z$ can be computed using Eq. (3) and (10). Two parameters are used to refer to the atmospheric water vapour content, these are Integrated Water Vapour (IWV) in units of kgm^{-2} which refers to the quantity of the atmospheric water vapour over a specific location and Precipitable Water (PW) is used to express the height of an equivalent column of liquid water in units of length. Bevis et al. (1992) gives IWV as

$$IWV = \int_0^\infty p_v(h)dh = \frac{1}{R_w}\int_0^\infty \frac{e(h)}{T(h)}dh \tag{11}$$

where p_v is the partial density of water vapour in kg/m^3; the height h in metres and R_w is the specific gas constant for water vapour in J/(kgK). PW relates to IWV by diving with the density of liquid water, ρ_w. $PW = IWV/\rho_w$. Again IWV is related to the ZWD using a dimensionless quantity as conversion factor, Π:

$$IWV = \frac{\Delta L_w^z}{\Pi}, \quad PW = \frac{\Delta L_w^z}{\rho_w \cdot \Pi} \tag{12}$$

From Eq. (5) and considering the second and third terms of Eq. (7), the wet delays become:

$$\Delta L_w^z = 10^{-6}\int_z (k_2^{'}\frac{e(z)}{T(z)} + k_3\frac{e(z)}{T(z)^2})dz \tag{13}$$

substituting the constants and introducing a mean temperature, T_m , which is defined by Bevis et al. (1992) as: $T_m = 0.72T_s + 70.2$, where T_s is the surface temperature. The conversion factor finally becomes:

$$\Pi = 10^{-6}\rho_w R_w(k_2^{'} + \frac{k_3}{T_m}) \tag{14}$$

Bevis et al. (1994) computed Π to be approximately 0.15, but this dimensionless constant is a function of season, location, and weather. The minimum and maximum values can have a range with variation of over 20% (Liou et al., 2001). For this study, 0.1629 was used for Π.

3 Data Processing

GPS data were processed using gLAB® (Hernandez-Pajares et al., 2010) software in Precise Point Positioning (PPP) mode and the estimate the ZTD values. The processing stages were:

1. Acquisition of GPS and surface meteorological data;
2. Precise receiver and orbit positions obtained from global GNSS analyses centres;
3. . Eliminate ionosphere effect;
4. Introduce (Phase center correction values, Ocean Tide effects, Relativistic corrections...) and
5. Finally estimate Zenith Path Tropospheric Delay which is used to derive IWV and PW

3.1 gLAB Software

gLAB® has been developed at the Research group of Astronomy & Geomatics at the Technical University of Catalonia in Barcelona, Spain. It is a multi-purpose package that runs on Windows and Linux operating systems and used to process and analyse GNSS data. The license is free on an "as is" basis without warranties or conditions of any kind. gLAB is a complete GNSS analysis tool for both educational and professional purposes. gLAB allows a full customization of its options and provides precise point positioning capabilities on the centimetre level. The software is able to output solutions of different application parameters including receiver position, satellite position and velocities, Satellite-receiver geometric distances, corrections to Satellite and receiver clocks, Relativistic Clock Correction, Wind-up correction Troposphere nominal correction and delays, Ionosphere correction, Relativistic path range correction and Solid Tides Correction. Processing can be done in standard and precise point positioning mode for static and kinematic receivers. Backward filtering is also supported to reduce errors associated with solution convergence. gLAB offers three different modules for processing:

1. Data Processing Core (DPC) - For all the processing
2. Graphic User Interface (GUI) - To customize options
3. Data Analysis Tool (DAT) - Graphics

Sample screenshots of the software during execution is shown in Fig. 3. Both the processing core and the plotting tool can be executed independently from the GUI. The latest release is gLAB version 2.0.0 in the year 2010 (Hernandez-Pajares et al., 2010).

Figure 3: gLAB Interface

3.2 KNUST GPS Station

A Sokkia® GSR 2600 18 channeled receiver and a SOK600 antenna mount on the roof of the New Engineering block was use to log data for the study. The station has been logging data since March 2013, with a three month break from June to August. The precise coordinates of the antenna position as computed using the gLAB® software is shown in Table 1.

Table 1: Base Station Coordinates

	ITRF 08		WGS 84		UTM (30N)	
KNUST Base	X	6333147.7330 ±0.0022	Φ	6°40′21.69989″	E	658546.074
	Y	-173104.4837 ±0.0009	Λ	−1°33′56.45069″	N	737797.244
	Z	736229.3232 ±0.0004	h_{ellip}	296.345		

In accepting the ZTD values computed with gLAB, a comparison with International GNSS Service (IGS) ZTD products and gLAB derived values for the IGS station in Yamoussoukro, Cote d'Ivorie[2] was done. Figure 4 show plots of ZTD values against time of day for some selected days in October, 2013, and Table 2 give results of descriptive statistics run on the two ZTD values. With the exception of the different software used (i.e. IGS analysis centres use GIPSY and Bernese software (Byun and Bar-Sever, 2009; Dach et al., 2007; Bohm et al., 2006)), similar parameters were used for data processing. The parameters were an elevation cut-off of 7°, simple nominal tropospheric correction and Niell mapping functions (hydrostatic and wet), 24 hour data time span and 300 secs data rate were implemented in gLAB. Others were precise orbits and clocks products and corrections due to Earth orientation and antenna phase center.

Considering the plots in Fig. 4, the initial differences in the ZTD values from gLAB are due to time delay in resolving all ambiguities in the phase solutions. Again the differences observed in the plots of the two datasets can

Table 2: Descriptive Statistics run on ZTD values from IGS servers and gLAB results

DoY	275		277		279	
	IGS	gLAB	IGS	gLAB	IGS	gLAB
Mean	2.5472	2.5458	2.5874	2.5772	2.5539	2.5461
Std Dev	0.0073	0.0044	0.0089	0.0050	0.0094	0.0063
Min	2.5387	2.5463	2.5648	2.5662	2.5281	2.5326
Max	2.5693	2.5574	2.6111	2.5892	2.5807	2.5637

DoY	281		282		285	
	IGS	gLAB	IGS	gLAB	IGS	gLAB
Mean	2.5465	2.5416	2.5563	2.5452	2.5607	2.5532
Std Dev	0.0163	0.0190	0.0246	0.0219	0.0149	0.0103
Min	2.5398	2.5242	2.5049	2.5104	2.5239	2.5376
Max	2.5647	2.5744	2.5988	2.5833	2.5957	2.5795

DoY	287		289	
	IGS	gLAB	IGS	gLAB
Mean	2.5021	2.4904	2.5489	2.5359
Std Dev	0.0189	0.0142	0.0203	0.0213
Min	2.4585	2.4675	2.5061	2.4978
Max	2.5450	2.5282	2.5872	2.5588

be attributed to the different approaches in ZTD computations, gLAB uses PPP techniques as opposed to differential/baselines from the IGS servers. From the results in Table 2, and correlation coefficients ranging between 0.893 – 0.916 the computed ZTD values from gLAB compares favourably with that of from IGS Servers. Hence, ZTD values from gLAB can be used for our study and analysis.

4 PW Comparison

The Precipitable Water (PW) values computed using the methodology and models described above were compared with global Re-analysis data from National Centers for Environmental Prediction (NCEP) and European Centers for Medium Range Weather Forecast(ECMWF) Era-Interim (Fig. 5). Correlation analyses were run and resulting, r, values of 0.839 for gLAB and ERA-Interim and 0.729 for gLAB and NCEP. The PW values computed with gLAB correlates better with ERA-Interim as opposed to NCEP. Figure 6 shows the correlation plots of computed PW for KNUST and values extracted from ERA-Interim and NCEP global reanalysis data. The correlation coefficients of this study gave values higher than those obtained for similar exercises across the African region. Bock et al. (2007) worked on comparing PW values computed from 9 International GNSS service stations across Africa with global re-analysis, radiosondes and AERONET data spanning a 3-year period, an averaged r values of 0.81 and 0.67 were obtained for ERA-40 and NCEP respectively. They further identified that the standard deviation, σ, decreases and correlation increases when the averaging period for data samples increases. These results clearly show that more

2 Yamoussoukro Tracking Station, YKRO, with IERS DOMES number of 32601M001 (http://igscb.jpl.nasa.gov/network/site/ykro.html)

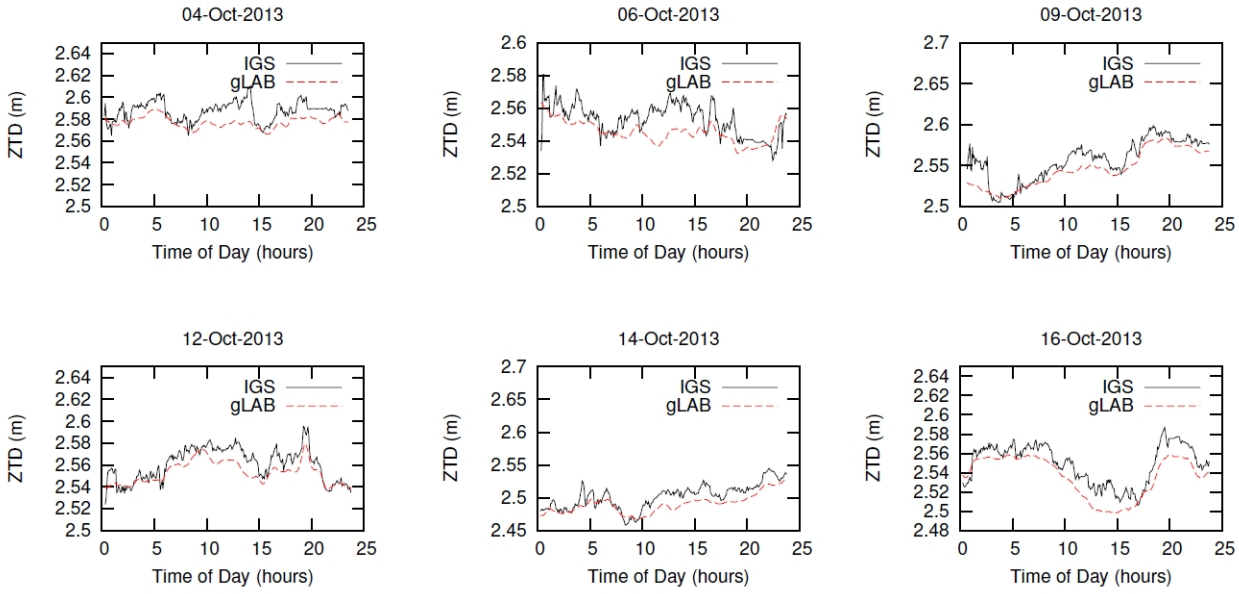

Figure 4: ZTD plot against Time-of-day for IGS server values and gLAB computations for Yamoussoukro, Cote d'Ivorie

work has to be done to indicate whether the global reanalysis models are oversampling or under-sampling precipitable water over Ghana. Similar assignments have been carried out in the past (Mims et al. (2011); Bokoye et al. (2003); Motell et al. (2002); Yoshihara et al. (2000)) all geared towards the comparisons of PW values retrieved from GPS, radiosonde, sun photometers, radiometers and other sensing approaches. Their concluding remarks show higher correlation for GPS against the conventional methods and thus proves that GPS offer a cheaper and accurate alternative in sensing water vapour.

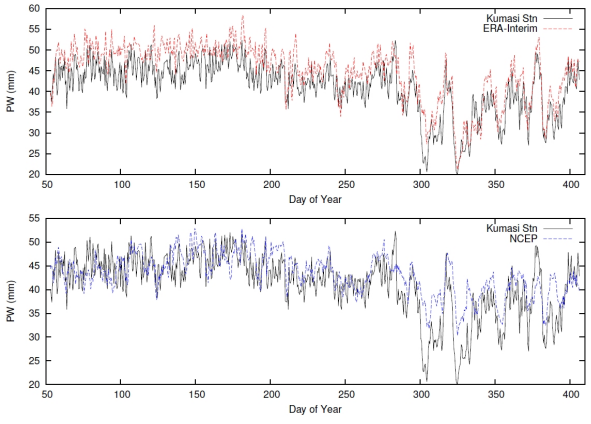

Figure 5: A plot of PW computed from gLAB, ERA-Interim and NCEP Reanalysis data against Day of Year ranging from March, 2013 to May, 2014

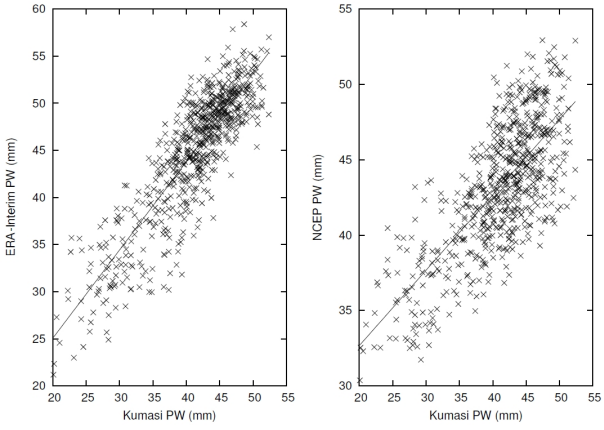

Figure 6: Correlation plots of computed PW for KNUST against ERA-Interim and NCEP global reanalysis data

To improve weather prediction and precipitation forecasting, this study proposes a collaborative effort between Ghana Meteorological Agency (GMet) and the Survey and Mapping Division of the Lands Commission of Ghana to adopt GNSS meteor. This concept can serve dual purpose of providing precise coordinates, differential corrections for PNT applications as well as PW for uploads into NWP servers. To deploy a system using a network of GNSS receivers to sense water vapour, 1° resolution in horizontal plane (approximately 110 km) for Ghana was considered. Again, GNSS meteorological concepts require surface data – pressure and temperature, for computation of PW. Merging these two assumptions and using the locations of GMet

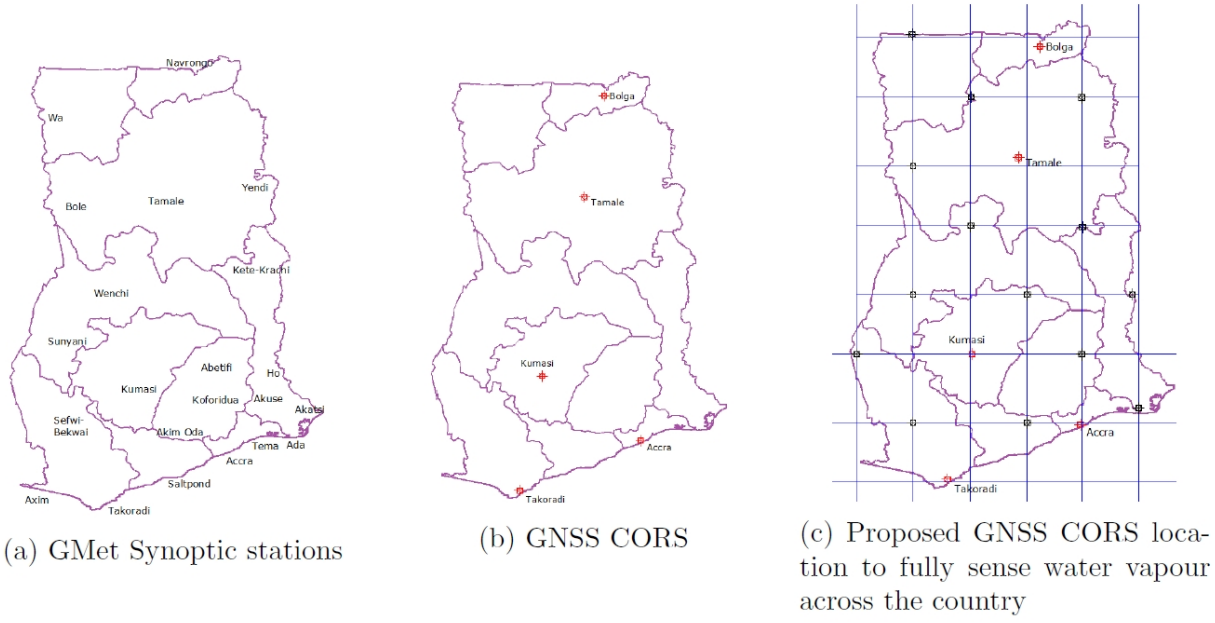

(a) GMet Synoptic stations (b) GNSS CORS (c) Proposed GNSS CORS location to fully sense water vapour across the country

Figure 7: GNSS Meteorological Set-up in Ghana

synoptic stations and GNSS continuously operating Base Stations as shown in Fig. 7. In all a minimum of 19 GNSS receivers will be enough to cover the whole nation.

5 Conclusion

At such an early stage in the project, this paper has outlined the procedures in retrieving Precipitable Water from GPS Base station data. The gLAB software implements algorithms that compute the ZTD values based on PPP techniques, precise clocks and orbit products. Initial results from this study that compared retrieved PW from GNSS and reanalysis products clearly indicates good agreement between the two global reanalysis data. This study is not meant to conclude or recommend one reanalysis product over the other but to give an indication of its sampling of atmospheric parameters in our subregion. Results show a stronger correlation between ERA-Interim and gLAB retrieved PW estimates than NCEP Reanalysis over the study area. To affirm this position, more data needs to be logged and a longer time series considered.

Again, the study has a broader aim of using a network of continuously operation GNSS stations to map water vapour at high resolutions for operational weather prediction Ghana. The fullest potential of GNSS meteorology will be realized when these two state institutions, Survey and Mapping Division works closely with the Ghana Meteor Agency through data and knowledge sharing.

References

Bevis, M., Businger, S., Chiswell, S., Herring, T. A., Anthes, R. A., Rocken, C., and Ware, R. H., 1994, GPS meteorology: Mapping zenith wet delays onto precipitable water. J. Appl Met, 33(3):379-386.

Bevis, M., Businger, S., Herring, T., Rocken, C., Anthes, R., and Ware, R., 1992, GPS meteorology- remote sensing of atmospheric water vapor using the global positioning system. J. Geophy. Res. 97(D14):15787-15801.

Bock, O., Bouin, M. N., Walpersdorf, A., Lafore, J. P., Janicot, S., Guichard, F., and Agusti-Panareda, A., 2007, Comparison of ground-based GPS precipitable water vapour to independent observations and NWP model reanalyses over africa. Quart. J. Roy. Met. Soc., 133(629):2011-2027.

Bohm, J., Niell, A., Tregoning, P., and Schuh, H., 2006, Global mapping function (GMF): A new empirical mapping function based on numerical weather model data. Geophy. Res. Letters, 33(7).

Bokoye, A. I., Royer, A., O'Neill, N. T., Cliche, P., McArthur, L. J. B., Teillet, P. M., Fedosejevs, G., and Theriault, J-M., 2003, Multisensor analysis of integrated atmospheric water vapor over Canada and Alaska. J. Geophy. Res.: Atmospheres (1984-2012), 108(D15).

Bosy, J., Rohm, W., Sierny, J., and Kaplon, J., 2011, GNSS meteorology. TransNav-Int. J. Marine Navigat. Safety Sea Transport, pages 79-83.

Buizza, R., 2002, Chaos and weather prediction. European Centre for Medium-Range Weather, Internal Report; Meteorological Training Course, pages 1-28.

Byun, S. H. and Bar-Sever, Y. E., 2009, A new type of troposphere zenith path delay product of the Interna- tional GNSS service. J. Geod. 83(3-4):1-7.

Dach, R., Hugentobler, U., Fridez, P., Meindl, M., et al., 2007, Bernese GPS software version 5.0. Astronomical Institute, University of Bern, 640.

Davis, J., Herring, T., Shapiro, I., Rogers, A., and Elgered, G., 1985, Geodesy by radio interferometry: Effects of atmospheric modeling errors on estimates of baseline length. Radio Sci, 20(6):1593-1607.

De Haan, S. and Van Der Marel, H., 2008, Observing three dimensional water vapour using a surface network of GPS receivers. Atmospheric Chemistry and Physics Discussions, 8:17193-17235.

El-Rabbany, A., 2002, Introduction to GPS: the Global Positioning System. Artech House Publishers, Norwood. Elgered, G., Davis, J. L., Herring, T. A., and Shapiro, I. I., 1991, Geodesy by radio interferometry: Water vapor radiometry for estimation of the wet delay. J. Geophy. Res.: Solid Earth (1978-2012), 96(B4):6541-6555.

Gendt, G., Dick, G., Reigber, C. H., Tomassini, M., Liu, Y., and Ramatschi, M., 2003, Demonstration of NRT GPS water vapor monitoring for numerical weather prediction in Germany. J Meteo. Societ. Jap, 82(1B):360-370.

Hernandez-Pajares, M., Juan, J., Sanz, J., Ramos-Bosch, P., Rovira-Garcia, A., Salazar, D., Ventura-Traveset, J., Lopez-Echazarreta, C., and Hein, G, 2010, The ESA/UPC GNSS-lab tool (gLAB). In Proc. of the 5th ESA Workshop on Satellite Navigation Technologies (NAVITEC' 2010), ESTEC, Noordwijk, The Netherlands.

Leick, A., 2003, GPS satellite surveying. Wiley, New York.

Liou, Y-A., Teng, Y-T., Van Hove, T., and Liljegren, J. C., 2001, Comparison of precipitable water observations in the near tropics by GPS, microwave radiometer, and radiosondes. J. Appl. Met. 40(1):5-15.

Lynch, P., 2008, The origins of computer weather prediction and climate modeling. J. Computational Physics, 227(7):3431-3444.

Mims, F. M., Chambers, L. H., and Brooks, D. R., 2011, Measuring total column water vapor by pointing an infrared thermometer at the sky. Bull. Amer. Met. Soc., 92(10).

Misra, P. and Enge, P., 2011, Global Positioning System: Signals, Measurements and Performance Revised 2^{nd} Ed. Massachusetts: Ganga-Jamuna Press.

Motell, C., Porter, J., Foster, J., Bevis, M., and Businger, S., 2002, Comparison of precipitable water over Hawaii using AVHRR-based split-window techniques, GPS and radiosondes. Int. J. Remote Sensing, 23(11):2335-2339.

Niell, A. E., 1996, Global mapping functions for the atmosphere delay at radio wavelengths. J. Geophy. Res., 101(B2):3227-3246.

Nilsson, T., Bohm, J., Wijaya, D. D., Tresch, A., Nafisi, V., and Schuh, H., 2013, Path delays in the neutral atmosphere. In Atmospheric Effects in Space Geodesy, J. Bohm and H. Schuh (eds.), pages 73-136. Springer- Verlag Berlin Heidelberg.

Ning, T., 2012,. GPS Meteorology: With Focus on Climate Application. PhD thesis, Chalmers University of Technology. http://publications.lib.chalmers.se/records/fulltext/157389.pdf.

Pichelli, E., Ferretti, R., Cimini, D., Perissin, D., Montopoli, M., Marzano, F. S., and Pierdicca, N., 2010, Water vapour distribution at urban scale using high-resolution numerical weather model and space- borne SAR interferometric data. Nat. Hazards Earth Syst. Sci., 10:121-132.

Pierdicca, N., Rocca, F., Basili, P., Bonafoni, S., Cimini, D., Ciotti, P., Ferretti, R., Foster, W., Marzano, F., Mattioli, V., et al., 2009, Atmospheric water-vapour effects on spaceborne interferometric SAR imaging: data synergy and comparison with ground-based measurements and meteorological model simulations at urban scale. In Antennas and Propagation, 3rd EuCAP European Conference, 3443-3447.

Pottiaux, E., 2010, Sounding the Earth's Atmospheric Water Vapour Using Signals Emitted by Global Navi- gation Satellite Systems. PhD thesis, Department of Physics, Earth and Life Institute, Catholic University of Louvain.

Saastamoinen, J., 1972, Atmospheric correction for the troposphere and stratosphere in radio ranging satellites. Geophysical Monograph Series, 15:247-251.

Sahoo, S., Bosch-Lluis, X., Reising, S. C., and Vivekanandan, J., 2013, Spatial resolution and accuracy of re- trievals of 2D and 3D water vapor fields from ground-based microwave radiometer networks. In Radio Science Meeting, US National Committee of URSI

Schiller, T., 2006, GNSS meteorology on moving platforms. Advances and limitations in kinematic water wapor estimation. Inside GNSS, 1(3):56-60.

Seeber, G., 2003, Satellite geodesy: foundations, methods, and applications. de Gruyter.

Seidel, D. J., 2002, Water vapor: Distribution and trends. Encyclopedia of Global Environmental Change, John Wiley & Sons, Ltd, Chichester.

Shuman, F. G., 1978, Numerical weather prediction. Bulletin of the American Meteorological Society, 59:5-17.

Solomon, S., Qin, D., Manning, M., Chen, Z., Marquis, M., Averyt, K. B., Tignor, M., and Miller, H. L., 2007, Climate change 2007: The physical science basis. contribution of working group I to the fourth assessment report of the intergovernmental panel on climate change. The IPCC scientific assessment, page 996. Cambridge University Press, UK and USA.

Soos, A., 2010, Global warming and climate models. Oilprice.com. http://oilprice.com/The-Environment/Global-Warming/Global-Warming-And-Climate-Models.html Accessed on May 2014.

Thayer, G. D., 1974, An improved equation for the radio refractive index of air. Radio Sci. 9(10):803-807. USGS, 2011, Greenhouse gases. US Geodetic Survey Science Education Handout, http://education.usgs.gov/lessons/gases.pdf. Accessed on Feb 2014.

Yoshihara, T., Tsuda, T., and Hirahara, K., 2000, High time resolution measurements of precipitable water vapor from propagation delay of GPS satellite signals. EARTH PLANETS AND SPACE, 52(7):479-494.